processes

MDPI

Essay

Study on Brittleness Characteristics and Fracturing Crack Propagation Law of Deep Thin-Layer Tight Sandstone in Longdong, Changqing

Changjing Zhou [1], Zhonghua Sun [2,3], Yuanxiang Xiao [1], Guopeng Huang [2,3], Dan Kuang [1] and Minghui Li [2,3,4,5,*]

[1] Oil Gas Technology Research Institute, PetroChina Changqing Oilfield Company, Xi'an 710018, China; zhoucj_cq@petrochina.com.cn (C.Z.); xiaoyx_cq@petrochina.com.cn (Y.X.); kdan_cq@petrochina.com.cn (D.K.)
[2] Institute of Unconventional Oil and Gas Science and Technology, China University of Petroleum (Beijing), Beijing 102249, China; szhcupb@163.com (Z.S.); hgpcupb@163.com (G.H.)
[3] State Key Laboratory of Petroleum Resources and Prospecting, China University of Petroleum (Beijing), Beijing 102249, China
[4] Oil & Gas and New Energy Branch, PetroChina Corporation, Beijing 100010, China
[5] Research Institute of Petroleum Exploration & Development, PetroChina Corporation, Beijing 100083, China
* Correspondence: lmhcupb@163.com

Abstract: Tight-sandstone oil and gas resources are the key areas of unconventional oil and gas resources exploration and development. Because tight-sandstone reservoirs usually have the characteristics of a low porosity and ultralow permeability, large-scale hydraulic fracturing is often required to form artificial fractures with a high conductivity to achieve efficient development. The brittleness of rock is the key mechanical factor for whether fracturing can form a complex fracture network. Previous scholars have carried out a lot of research on the brittleness characteristics of conglomerate and shale reservoirs, but there are few studies on the brittleness characteristics of sandstone with different types and different coring angles in tight-sandstone reservoirs and the fracture propagation law of sandstone with different brittleness characteristics. Based on this, this paper carried out a systematic triaxial compression and hydraulic fracturing experiment on the tight sandstone of Shan 1 and He 8 in the Longdong area of the Changqing oilfield. Combined with CT scanning cracks, the brittleness characteristics and fracturing crack propagation law of different types and different coring angles of sandstone under formation-confining pressure were clarified. The results show that there are great differences between different types of sandstone in the yield stage and the failure stage. The sandstone with a quartz content of 100% has the highest peak strength and a strong brittleness. Sandstones with a high content of natural fractures and dolomite have a lower peak strength and a weaker brittleness. There are also differences in the peak strength and fracture morphology of sandstone with different coring angles due to geological heterogeneity. The sandstone with a comprehensive brittleness index of 70.30 produces a more complex fracture network during triaxial compression and hydraulic fracturing than the sandstone with a comprehensive brittleness index of 14.15. The research results have important guiding significance for on-site fracturing construction of tight-sandstone reservoirs.

Keywords: tight sandstone; triaxial compression; brittleness characteristics; hydraulic fracturing; fracture propagation

Citation: Zhou, C.; Sun, Z.; Xiao, Y.; Huang, G.; Kuang, D.; Li, M. Study on Brittleness Characteristics and Fracturing Crack Propagation Law of Deep Thin-Layer Tight Sandstone in Longdong, Changqing. *Processes* **2023**, *11*, 2636. https://doi.org/10.3390/pr11092636

Academic Editors: Hadi Jabbari and Vamegh Rasouli

Received: 29 July 2023
Revised: 28 August 2023
Accepted: 30 August 2023
Published: 4 September 2023

1. Introduction

Tight-sandstone oil and gas reservoirs are the key areas for the exploration and development of unconventional oil and gas resources [1–3]. The Longdong area of Ordos Basin has good oil generation and storage conditions, and tight-sandstone oil and gas resources are very rich. The detailed geological characteristics of the study block can be found in [4–8]. Tight reservoirs have the characteristics of a low porosity and a low permeability, and single wells often have no natural industrial production capacity. Existing

research and a large number of engineering practices have shown that for tight sandstone reservoirs, the formation of a complex fracture network with a high conductivity near the wellbore through large-scale volume fracturing technology is the key to achieving efficient development of such reservoirs [8]. Therefore, whether it can break the reservoir and form a complex artificial fracture network in the near wellbore area during fracturing construction has become the focus of research. At present, scholars generally believe that the volume fracturing effect is related to the rock mechanical characteristics of the reservoir, the development degree of natural fractures and the in situ stress. The mechanical brittleness of rock is the key mechanical parameter to evaluate the effect of volume fracturing. The higher the brittleness index is, the easier it is for the reservoir to form a complex fracture network in the process of hydraulic fracturing, and the better the reservoir reconstruction effect is [9,10]. Due to the influence of the sedimentary environment and diagenesis, tight-sandstone reservoirs usually have the characteristics of large changes in rock types and a strong heterogeneity, resulting in large differences in brittleness characteristics of different downhole tight-sandstone reservoirs in the same block [11]. Therefore, it is of great guiding significance to study the brittleness characteristics and fracture propagation law of different downhole tight-sandstone reservoirs in the Longdong area of Ordos Basin for the effective development of tight-sandstone reservoirs in the Changqing oilfield.

In recent years, scholars have carried out a lot of research on rock brittleness characteristics and established a large number of rock brittleness index evaluation models [12,13]. However, at present, there is no uniform standard for the calculation of a rock brittleness index, which is generally summarized into three aspects: (1) The brittleness index is defined based on the mineral composition of the rock. The content of brittle minerals in the rock is determined by an XRD experiment, and the brittleness index is calculated. However, this method does not consider the influence of mechanical characteristics and geological effects on rock brittleness. Based on the analysis of mineral composition, mechanical parameters and energy evolution characteristics of previous scholars, Shi et al. (2022) proposed a new brittleness evaluation method for the Lucaogou Formation's oil and gas reservoirs. The results showed that the brittleness characteristics of different lithology rocks in the Lucaogou Formation of Jimsar were quite different [14]. (2) Based on the rock mechanics' parameters, the brittleness index is defined, and the brittleness index is calculated by considering the elastic modulus and Poisson's ratio. This method is currently used more. Based on field logging data, Xiao (2022) combined the field logging data of the longitudinal wave time difference, using the formula to calculate the shear wave time difference, and then obtain the Young's modulus and Poisson's ratio, etc. The mechanical parameters of different wells in the Yingtai area were studied. Through the calculation of rock mechanics' parameters, the rock brittleness index curve in the longitudinal direction of the formation was obtained. At the same time, the reliability of the calculation results was verified by the triaxial compression experiment of the core, and the conclusion that the rock with a high brittleness index was more likely to produce cracks in the fracturing process was put forward [15]. (3) The brittleness index is defined based on the complete stress–strain curve of rock during triaxial compression. However, the current calculation method needs to provide the stress–strain curve of the whole process of triaxial compression to obtain parameters such as residual strain. However, during the experiment, the rock is broken after the peak strength point, which often makes the stress–strain curve after the peak strength difficult to obtain, thus limiting the application of this method. Gao et al. (2022) proposed a brittleness evaluation method based on the characteristics of stress–strain curves before and after the peak strength of rock triaxial compression. First, combined with the definition of brittleness characteristics by previous scholars, the feasibility of a brittleness evaluation method based on the characteristics of the stress–strain curve before and after the peak strength of rock triaxial compression was analyzed theoretically. Second, the brittle component Bi before the peak strength and the brittle component Bii after the peak strength were constructed, and the product of Bi and Bii was used as the brittleness index BI to characterize the characteristics of the full stress–strain curve [16]. Meng et al., studied

the development and role of rock brittleness in different fields of rock engineering. The 80 brittleness indexes published in the literature of rock mechanics were recorded, and the measurement methods, applicability and limitations of some indexes were discussed. Among the indicators reviewed, the indicators based on stress–strain curves accounted for the majority, followed by indicators based on strength parameters, mineral composition, elastic parameters and conventional logging data [17]. In this paper, the brittleness index was calculated based on the method of rock mechanics' parameters. The normalized numerical model considering Poisson's ratio and elastic modulus parameters and the secant modulus model of peak strength were used to evaluate the brittleness characteristics of 18 downhole cores in the Longdong area.

After the evaluation of the brittleness characteristics of different downhole cores, it is necessary to further optimize the downhole cores with different brittleness indexes for fracturing crack propagation experiments. The true triaxial hydraulic fracturing experiment is an effective means to understand the crack propagation law of tight sandstone with different brittleness characteristics. At present, a large number of scholars have studied the fracture propagation of hydraulic fracturing in sandstone and shale reservoirs [18–21]. Li et al. (2022) quantitatively studied the multifracture propagation morphology in the process of temporary plugging and diverting fracturing through true triaxial hydraulic fracturing experiments and CT scanning experiments and studied the key fracturing parameters such as perforation cluster spacing, perforation cluster number, fracturing fluid viscosity and in situ stress [22]. However, few scholars have carried out hydraulic fracturing experiments on downhole tight-sandstone cores with different brittleness indexes. Kong et al. (2023) carried out triaxial fracturing experiments on tight-sandstone samples by using 30 cm × 30 cm × 30 cm true triaxial hydraulic fracturing experimental equipment. At the same time, the fracture morphology was quantitatively characterized, and the fracture propagation law of tight-sandstone rock samples was studied in combination with the pressure curve. The research results showed the influence of natural fractures, horizontal two-way stress difference, fracturing fluid system and injection displacement on fracture propagation during hydraulic fracturing and clarified the influence of engineering parameters on fracture propagation and complex fracture network formation during hydraulic fracturing [23]. Jin et al. (2021) explored the influence of temporary plugging fracturing on crack initiation and propagation through true triaxial hydraulic fracturing experiments. The results showed that multiple temporary plugging fracturing could generate branch cracks on the basis of initial cracks, forming complex fracture networks, and increasing construction displacement during temporary plugging fracturing could form more cracks. The fracture initiation pressure of perforation completion was lower than that of open hole completion, and the fracture propagation direction was biased toward the maximum stress direction. The viscosity of fracturing fluid could significantly increase the rock fracture pressure [24].

Therefore, this study comprehensively considered the brittleness characteristics of sandstones with different types and different coring angles in the Longdong area and carried out triaxial compression experiments under in situ stress. At the same time, based on the normalized numerical model of Poisson's ratio and elastic modulus parameters and the secant modulus model of peak strength, the brittleness characteristics of 18 downhole cores in Longdong area were quantitatively evaluated. Combined with CT scanning experiments, the fracture morphology of triaxial compression was reconstructed. Finally, true triaxial hydraulic fracturing experiments were carried out on downhole cores with different brittleness indexes, and the influence of the brittleness index on the fracture propagation law of true triaxial hydraulic fracturing was explored. The research results have important guiding significance for the optimization of geological engineering deserts and on-site fracturing construction in the Longdong area of the Changqing oilfield.

2. Methodology

2.1. Experimental Samples

In this study, the tight sandstone was taken from the Shan 1 and He 8 sections in the Longdong area of the Changqing oilfield. The Shan 1 and He 8 members are located in the Su 76 and Su 25 blocks, which are located in the northeast and east of the north part of Sulige gas field, respectively. The administrative regions are subordinate to Etuoke Banner and Wushen Banner of Ordos City, Inner Mongolia Autonomous Region. The sampling depth was 3700–4400 m. A cylindrical sample with a diameter of 25 mm and a length of about 70 mm and a full-diameter core with a diameter of 100 mm and a length of about 120 mm were drilled from 18 wells, and then the samples were cut and processed. The cylindrical samples were processed into standard cores, and the full-diameter cores were poured into 100 × 100 × 100 mm samples with epoxy resin AB glue using a membrane for the true triaxial hydraulic fracturing experiments. In order to truly simulate the influence of perforation holes, we cut three grooves with a depth of 8 mm in the open hole section of the wellbore.

Gravel sandstone is a loose gravel sand structure. The size of the gravel is 2–5 mm, subround and subangular. The composition of gravel is mainly siliceous, and the content of gravel is about 5%. The sand debris is composed of feldspar, quartz and rock debris, with a size of 0.06–2 mm and a poor sorting. The color of gray sandstone is usually gray or light gray, the particle size is generally fine, and the sand particle diameter is between 0.0625 and 2 mm. The structure is usually a layered structure, and there are obvious bedding and parallel arrangement characteristics between sand particles. The main mineral components include quartz, feldspar, mica, etc., of which quartz is the most important component. White sandstone has a white or light gray color, which is formed due to the accumulation and compaction of sand and gravel particles. White sandstone is mainly composed of quartz particles, and may also contain a small amount of feldspar, mica, iron oxide and so on. White sandstone usually presents a homogeneous structure, and the particles are closely packed with a high density. Quartz sandstone is a kind of consolidated sandy rock, in which the content of quartz and siliceous rock debris is more than 95%. It usually contains little impurity matrix, and its chemical composition is simple, mainly silicon dioxide; the color is lighter; the roundness of the debris particles is good, and the sorting is good. Table 1 is the table of mineral composition test results of different downhole cores. It can be found that the quartz content of quartz sandstone reached 100%, and the quartz content of white sandstone also reached more than 90%. Some downhole cores showed the characteristics of dolomite, for example, the dolomite content of the 2-11-34 sample was higher; the quartz content of gray sandstone and pebbly sandstone was slightly lower. According to the above classification, the main rock types obtained from field sampling were pebbly sandstone, gray sandstone, white sandstone and quartz sandstone, as shown in Figure 1. In Figure 1(2e,2f), it can be seen that the surface of the core 3-25-11 was uneven, forming multiple surface dissolution cracks; core 1-14-55 formed a natural fracture in the middle of the core.

Table 1. Test results of mineral components in different downhole cores.

Rock Type	Sample	Mineral Content (%)						
		Quartz	Plagioclase	Calcite	Dolomite	Mixed-Layer Illite	Illite	Chlorite
Silicarenite	3-16-41	100.0						
Malmstone	1-13-70	82.6	4.4	4.8		2.7	3.4	2.1
	1-15-90	87.7				3.7	5.7	3.3
White Sandstone	2-11-34	5.1			94.9			
	1-13-65	94.5		5.5				
	54-6-49	94.3		5.7				
Pebbled Sandstone	1-22-18	87.9		12.1				
	1-12-54	84.7		12.1		1.1	1.5	0.6

(1)

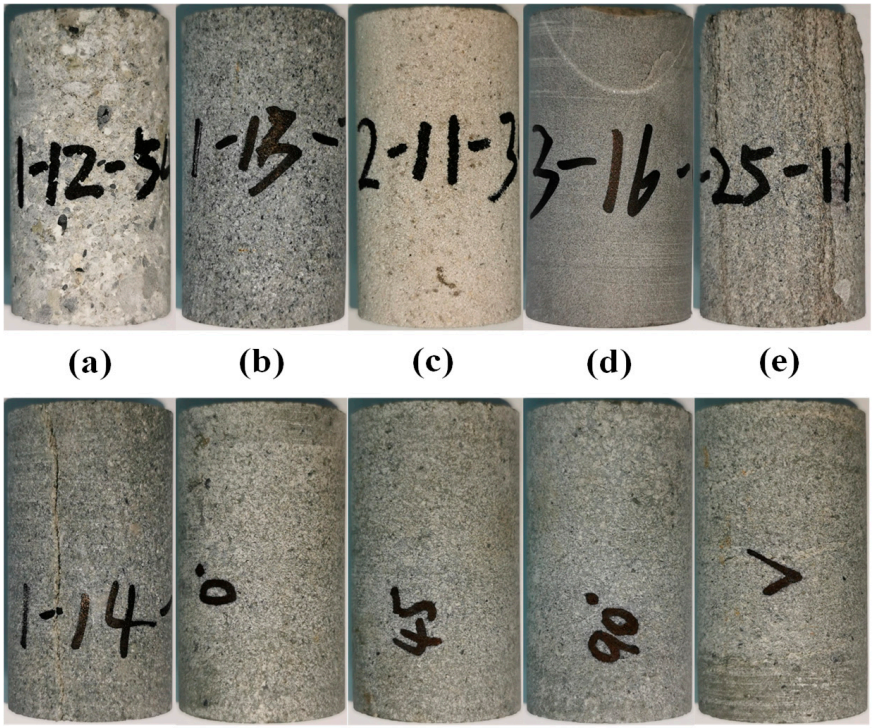

(a) (b) (c) (d) (e)

(f) (g) (h) (i) (j)

(2)

Figure 1. *Cont.*

(3)

Figure 1. Pictures of different sandstone types in the Shan 1 and He 8 sections in the Longdong area. (**1**) Seventeen different downhole core photos; (**2**) photos of different types of sandstone; (**a**) pebbly sandstone; (**b**) gray sandstone; (**c**) white sandstone; (**d**) quartz sandstone; (**e**,**f**) sandstones with natural fractures; (**g**) horizontal direction of the core angle of 0° sandstone; (**h**) sandstone with a horizontal coring angle of 45°; (**i**) sandstone with a horizontal coring angle of 90°; (**j**) sandstone cored perpendicular to the formation direction; (**3**) full-diameter core photos for the experiment.

The main rock types obtained from field sampling were pebbly sandstone, gray sandstone, white sandstone and quartz sandstone, as shown in Figure 1. The porosity of the 21 downhole cores was between 2.2 and7.1% and the permeability was between 0.01 and 0.12 mD, determined by using a gas porosity meter and a permeability meter. XRD test results showed that quartz sandstone had the highest proportion of quartz, which was 100%. The proportion of quartz in white sandstone was second, reaching more than 90%. The content of quartz in pebbly sandstone and gray sandstone was the lowest, accounting for about 80%. In addition, gray sandstone also contained about 10% of clay minerals.

2.2. Experiment Equipment

2.2.1. TAR-1500 Hydraulic Servo Experimental Test System

In this study, the TAR-1500 hydraulic servo experimental test system was used to carry out the core triaxial compression experiment. As shown in Figure 2. The system can provide a maximum axial load of 400 kN, a confining pressure of 80 MPa and a pore pressure of 40 MPa. The system is equipped with an imported LVDT variant sensor, which can achieve the required measurement accuracy in various pressure test environments [25].

2.2.2. GE Brivo CT385 CT Scanner

GE Brivo CT385 CT scanner can scan the internal fracture morphology of rock samples after fracturing (Figure 3). The principle is that X-rays are absorbed and scattered when they pass through matter. Rock particles and fractures have different degrees of X-ray absorption and scanning, so fractures can be characterized. In this experiment, the scanned core sample was placed in the middle of the core holder, and an X-ray CT scan was performed from one side to the other side [25].

Figure 2. TAR-1500 hydraulic servo experimental test system.

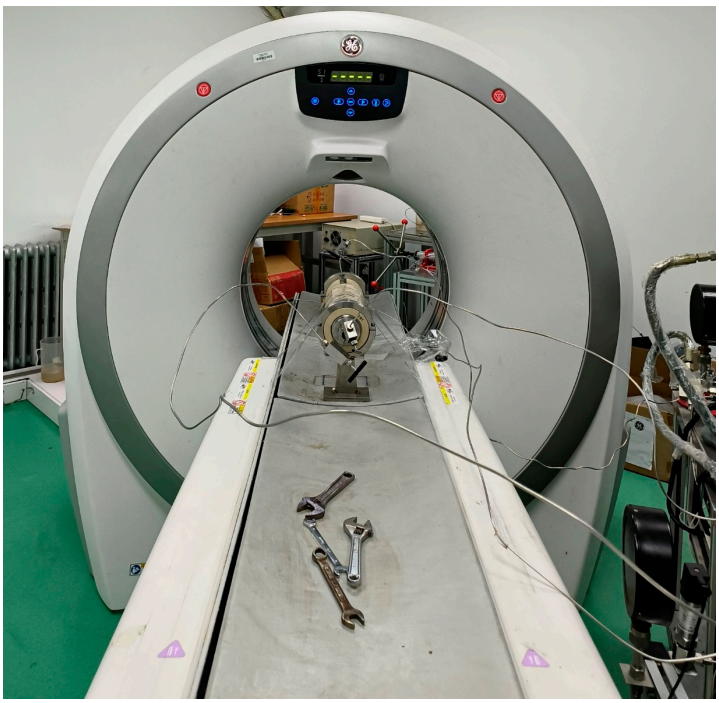

Figure 3. GE Brivo CT385 CT scanning device.

2.2.3. True Triaxial Hydraulic Fracturing Device

The true triaxial hydraulic fracturing device includes an ISCO pump, a pressure sensor, an intermediate container, a confining pressure pump and a rock chamber. In the process of the experiment, the fracturing fluid was put into the intermediate container, and the fracturing fluid was pumped into the rock sample through the ISCO pump. The confining

pressure pump could apply triaxial stress to the rock sample, the maximum triaxial stress was 30 MPa, the maximum pumping pressure of the ISCO pump was 70 MPa, and the maximum pumping flow rate was 204 mL/min. The pressure sensor could monitor the change in pumping pressure during the whole process of the experiment [22].

2.3. Experimental Scheme and Process

The field logging data showed that the formation pressure of the 4000 m reservoir depth in Longdong was about 40 MPa. In order to make the indoor experiment more accurately reflect the reservoir characteristics, we applied a confining pressure of 40 MPa to the triaxial compression experiment of 21 cores in 18 wells. After triaxial compression, the CT scanning device was used to scan the core after fracturing, and the CT data volume was imported into AVIZO software for a three-dimensional reconstruction of the digital core to obtain the spatial geometry of fractures. After that, the brittleness characteristics of all cores were quantitatively evaluated, and the full-diameter cores with different brittleness indexes were selected according to the brittleness evaluation results for true triaxial hydraulic fracturing experiments. The hydraulic fracturing experiments of high-brittleness-index and low-brittleness-index rock samples were carried out by a single factor analysis method. The displacement was set to 20 mL/min, the perforation cluster had 3 clusters, the fracturing fluid was guanidine gum fracturing fluid, and the horizontal stress difference was set to 2.5 MPa.

The specific experimental scheme was as follows: (1) We cut the core and measured the basic physical parameters. (2) According to the rock mechanics' parameters and stress–strain curve, the brittleness characteristics of the rock were analyzed. At the same time, the fracture propagation law in the three compression processes was studied according to the cores with different brittleness characteristics. (3) The cores with different brittleness indexes were selected for hydraulic fracturing experiments. After fracturing, the samples were scanned by CT to obtain the fracture propagation law of sandstone fracturing with different brittleness indexes. The specific experimental process is shown in Figure 4.

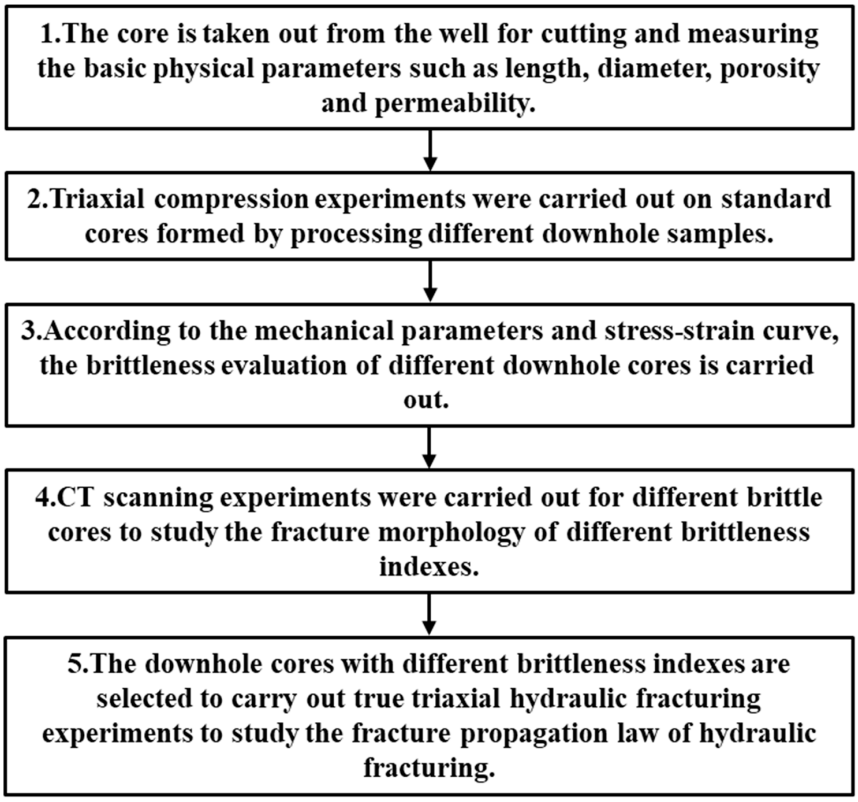

Figure 4. Experimental flow chart.

3. Results and Discussion

3.1. Evaluation of Mechanical Characteristics of Sandstone

In the triaxial compression experiment of rock, the increase in axial load will accumulate a large amount of energy inside the rock. At the same time, this energy will continuously destroy the pore structure inside the rock, which will increase the internal confusion of the rock. The stress expands to the edge and releases sharply to form cracks. The cumulative energy is also released at that time. The absorbed energy before and after the peak stress represents the ability of the rock at different loading stages. Before the peak stress, the absorbed energy represents the ability of the rock to accept the elastic energy of the applied load before the complete failure. After the peak stress, the absorbed energy represents the bearing capacity of the rock after the complete failure. It is also an important standard for the evaluation of a rock brittleness index [26].

The results of triaxial compression experiments in this study are shown in Table 2. In the triaxial compression experiment of 21 groups of 18 wells in Longdong area, the confining pressure of 40 MPa corresponding to the formation pressure was applied, but the mechanical parameters showed great differences. This shows that due to the existence of a formation heterogeneity, even if the reservoir rock is in the same block, its mechanical parameters will produce greater nonuniformity. The SEM scanning results of the core thin sections are shown in Figure 5, and it can be seen that the micropores and microfractures of the tight sandstone in Longdong are more developed.

Table 2. Triaxial compression test results table.

Core No.	Length (mm)	Diameter (mm)	Weight (g)	Density (g/cm^3)	Confining Pressure (MPa)	Compressive Strength (MPa)	Elastic Modulus (GPa)	Poisson Ratio
1-12-54	50.17	24.78	60.93	2.52	40	299.116	38.484	0.176
1-12-73	50.04	24.77	63.02	2.61	40	466.811	58.122	0.223
1-13-64	50.24	24.81	63.09	2.60	40	559.652	55.159	0.207
1-13-65	50.19	24.81	60.75	2.50	40	525.985	51.756	0.204
1-13-70	50.11	24.77	63.64	2.64	40	427.683	49.576	0.198
1-14-55	50.11	24.78	63.21	2.62	40	261.949	38.705	0.201
1-14-60	50.18	24.78	63.59	2.63	40	368.264	53.216	0.187
1-14-71	50.11	24.81	61.13	2.52	40	514.195	55.174	0.212
1-15-90	45.01	24.80	56.80	2.61	40	382.467	41.523	0.172
1-17-87	50.12	24.82	62.54	2.58	40	511.726	49.919	0.211
1-18-110	50.15	24.75	63.49	2.63	40	347.377	41.673	0.202
1-22-18	50.11	24.81	63.72	2.63	40	498.030	67.481	0.188
2-11-34	50.04	24.78	59.63	2.47	40	318.057	33.679	0.288
3-16-41	50.10	24.78	68.34	2.83	40	613.342	91.893	0.258
3-25-11	50.11	24.90	63.12	2.59	40	192.684	33.399	0.265
54-1-12	50.15	24.81	63.75	2.63	40	336.972	38.445	0.218
54-6-49	40.09	24.79	48.70	2.52	40	499.280	39.516	0.172
0°	50.15	25.13	66.97	2.69	40	556.162	67.025	0.148
45°	50.01	25.15	66.51	2.68	40	498.681	67.759	0.161
90°	50.14	25.05	66.31	2.68	40	579.245	69.152	0.208
V	50.13	25.15	66.76	2.68	40	557.187	64.714	0.153

3.1.1. Analysis of Stress–Strain Curves of Different Types of Sandstone

The stress–strain curve of 17 groups of different types of tight sandstone under a triaxial compression load is shown in Figure 6. It can be seen from Figure 6 that except for quartz sandstone, the compression curves of other sandstones have obvious compaction stages. This is because in the quartz sandstone, quartz accounted for 100%, and quartz has strong brittle characteristics, so it is difficult to compress. All rocks have three stages of elasticity, yield and failure. The stress–strain curves of the four kinds of sandstone in the elastic stage are basically the same, and the curves in the yield stage and the failure stage

are quite different. It is generally observed that the yield stage of gray sandstone is the most obvious. However, due to the influence of natural fractures and mineral components, there are also samples with longer yield stage in gravel sandstone and white sandstone, which show significant plastic failure characteristics [27]. Through triaxial compression experiments, Shi et al. (2021) obtained that the stress of sandstone core increased with the increase in strain during loading and decreased sharply after the peak stress value. When the stress decreases rapidly, the lower residual stress indicates that the bearing capacity of the rock after failure is low, and the brittle characteristics are weak. This is similar to the stress–strain curve characteristics and brittleness characteristics in this study [28].

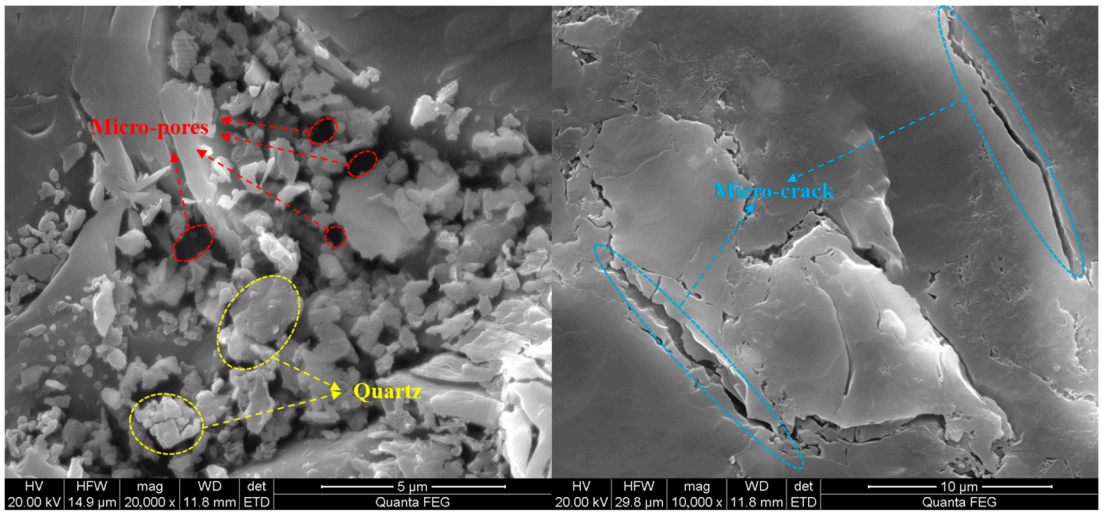

Figure 5. SEM image of Longdong tight sandstone.

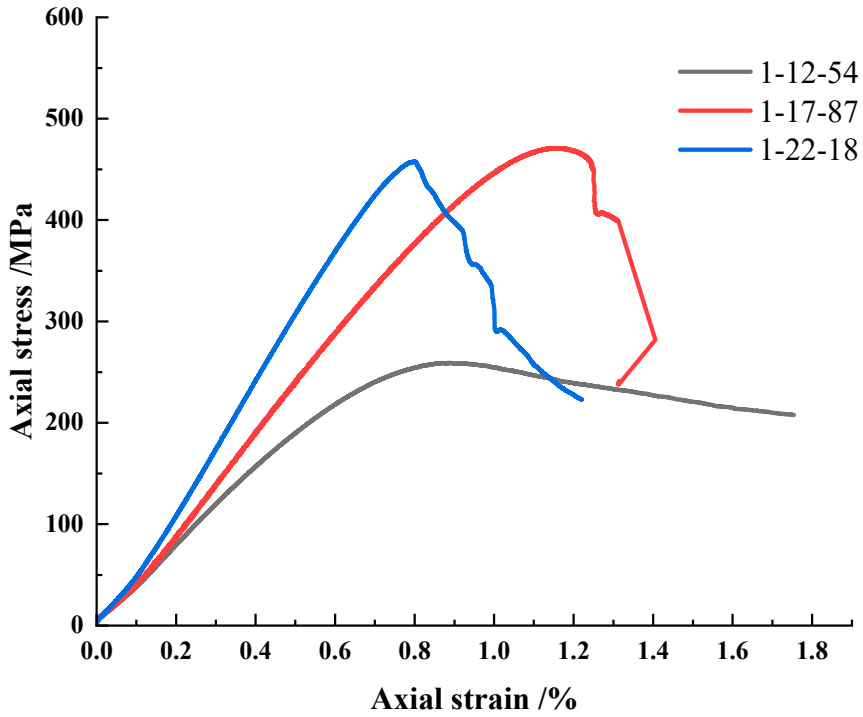

(**a**)

Figure 6. *Cont.*

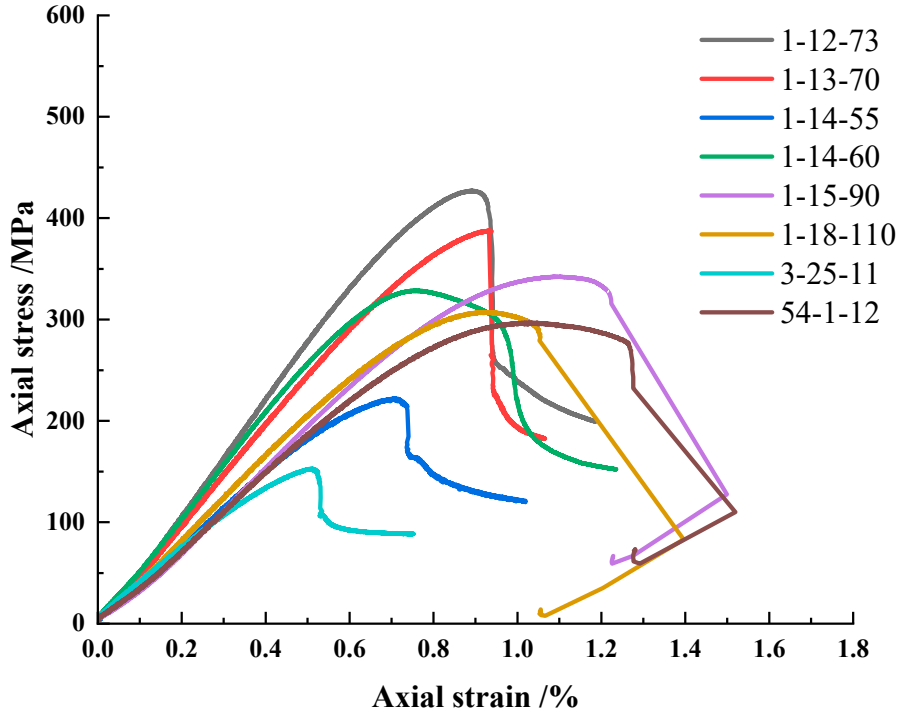

(**b**)

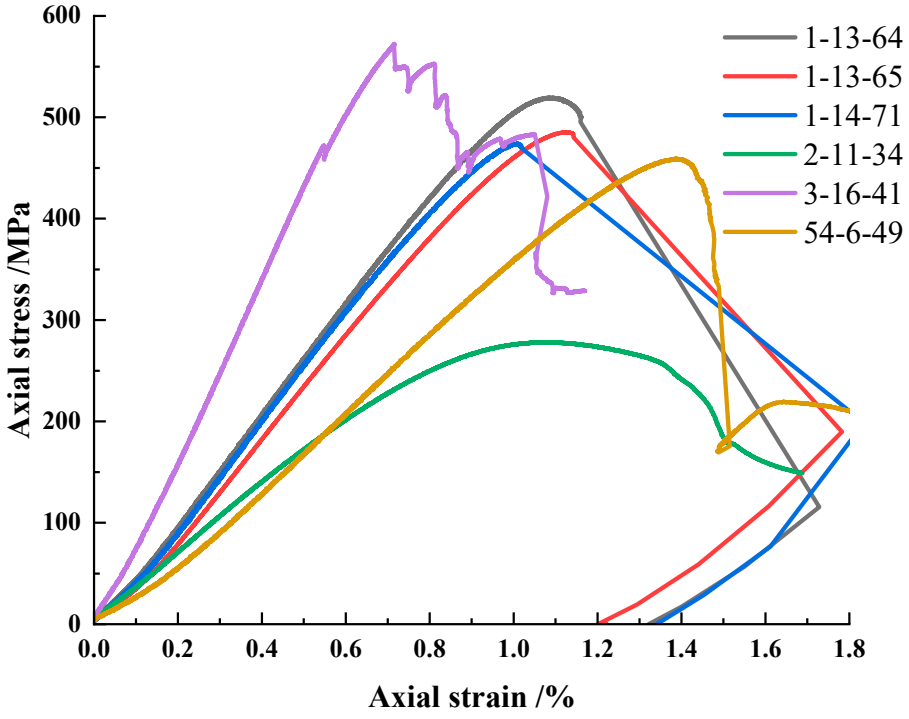

(**c**)

Figure 6. Stress–strain curves of different types of tight sandstone. (**a**) Stress–strain curve of pebbly sandstone; (**b**) stress–strain curve of gray sandstone; (**c**) stress–strain curves of white sandstone and quartz sandstone.

During the failure stage, the same type of sandstone also showed strong differences. The peak stresses of the 3-25-11, 2-11-34 and 1-12-54 samples were lower, which were 150.727 MPa, 271.684 MPa and 258.47 MPa, respectively. The analysis found that there were natural fractures in the 3-25-11 samples, and the presence of natural fractures reduced the peak strength. The content of dolomite in the mineral composition test of the 2-11-34 samples was higher, while the hardness of dolomite was lower, resulting in a lower peak strength. The 1-12-54 sample contained a large amount of gravel. There are usually large pores between quartz particles and gravel particles in gravel-bearing sandstone, which will lead to a decrease in the overall strength of the rock. In addition, the gravel particles themselves may have low strength, which will also affect the overall strength of gravel-bearing sandstone. The peak strength of quartz sandstone with 100% quartz was the highest at 572.268 MPa.

On the whole, the peak strength of white sandstone was generally higher than that of gray sandstone and pebbly sandstone. This is because the main component of white sandstone is quartz particles. Quartz has a high hardness and strong structure, which can withstand large stress and is not easy to break. The composition of gray sandstone contains a certain proportion of clay minerals, which are more fragile than quartz and will reduce the overall strength of the rock. Generally speaking, the strength of gravelly sandstone is relatively low. This is because there are usually large pores or voids between quartz particles and gravel particles in gravel-bearing sandstone, which will lead to a decrease in the overall strength of the rock. However, the peak strength of some pebbly sandstones in this study was also high. For example, the peak strength of the 1-17-87 samples was 470.808 MPa. We speculate that this may be related to the number, particle size and mineral composition of the gravels. Subsequent experiments will further verify this result.

The triaxial compression stress–strain curves of different types of sandstone cores in 17 wells of the Shan 1 and He 8 sections in the Longdong area showed great differences, which indicated a strong formation heterogeneity. At the same time, even the peak strength and postpeak stress drop rate of the same type of sandstone also showed obvious differences, which indicated that even for the same type of reservoir, its brittleness characteristics and compressibility also showed different characteristics. In the process of field fracturing construction, the petrological properties of the formation should be fully considered, and the double desert area of geological desert and engineering desert should be found for fracturing construction, so as to obtain a better oil recovery [29]. Zhu et al. (2023) obtained that the geological desert area was not necessarily a high oil and gas production area, and the high engineering desert area was not necessarily a high production area. Only by optimizing the coincidence area of double deserts could the oil and gas production be improved to the greatest extent, which is consistent with the research results of this paper [30].

3.1.2. Analysis of Stress–Strain Curves of Sandstone with Different Coring Angles

Previously, we analyzed the mechanical properties of 17 downhole cores from Shan 1 and He 8 in the Longdong area and concluded that the mechanical properties of different downhole cores in the block exhibited strong differences. Based on this, we conducted triaxial compression experiments on cores with different angles drilled in the same well to explore the mechanical properties of cores with different coring directions in the same well. A vertical rock sample (V) perpendicular to the formation direction was drilled from a vertical well in the field, and a rock sample (0°, 45°, 90°) was drilled at 45° intervals in the vertical formation horizontal plane. A total of four samples were drilled for the experiments. The results are shown in Figure 7. It can be seen from the stress–strain curve that there is little difference in the shape of the prepeak and postpeak curves of samples with different coring angles, indicating that the brittleness characteristics of the same downhole core are similar. However, there are some differences in peak intensity. The peak intensity of the 45° core of the horizontal sample is the lowest, and the peak intensity of the 90° core of the horizontal sample is the highest, which indicates the anisotropy of

the formation sedimentary development. Through a variety of experimental methods, Yuan et al. (2023) also obtained that the outcrop tight-sandstone reservoir had a serious stratigraphic heterogeneity from bottom to top in the vertical direction. This is similar to the heterogeneity of the reservoir in different directions studied in this paper [31].

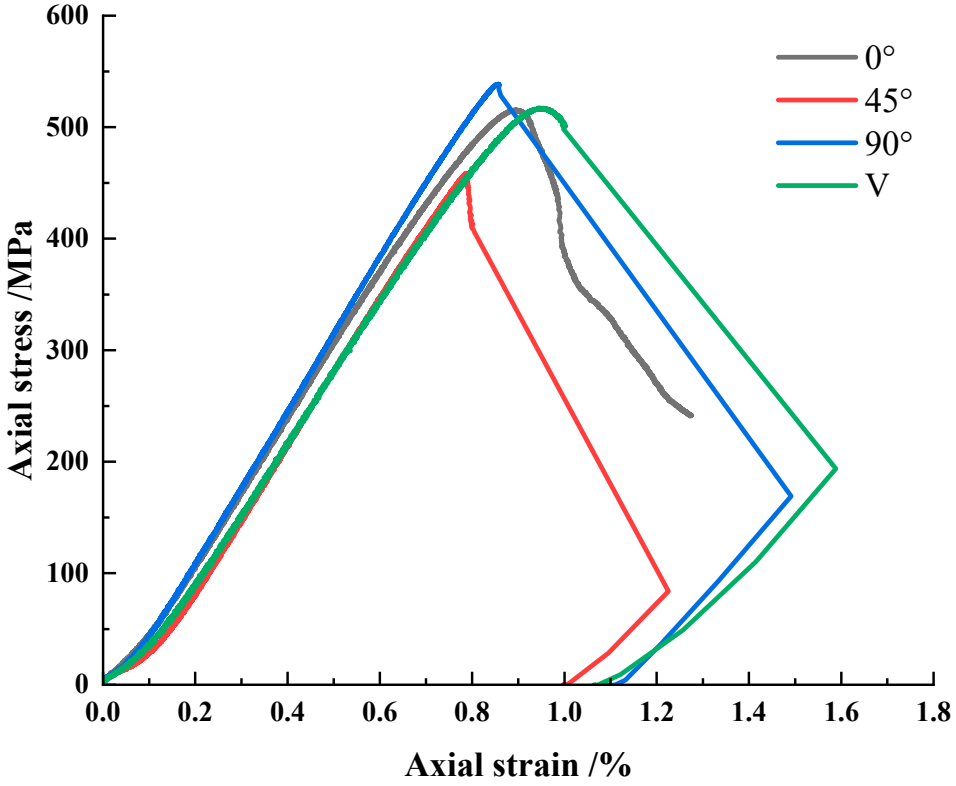

Figure 7. Stress–strain curves of sandstone with different coring angles in the same well.

3.2. Quantitative Evaluation of Sandstone Brittleness Index

According to the theory of rock mechanics, brittleness refers to the nature of rock internal deformation and fracture under load loading. The brittleness of rock in the process of hydraulic fracturing has an important influence on the fracturing effect. If the brittleness of reservoir rock is good, it is easier to form a complex fracture network in the process of hydraulic fracturing, so as to improve the oil recovery. On the contrary, the brittleness of reservoir rock is poor, and hydraulic fracturing has difficulties producing a complex fracture network, which reduces the range of reservoir stimulation. In view of the characteristics of a strong reservoir heterogeneity, complex sandstone types and natural fractures in the Longdong area, we used two models based on Poisson's ratio, a normalized numerical model of elastic modulus parameters and the secant modulus of the peak strength to quantitatively evaluate the brittleness index of 21 different downhole cores in the Longdong area.

Generally speaking, the greater the elastic modulus, the lower the Poisson's ratio, the stronger the brittleness. The Poisson's ratio can reflect the ability of rock to initiate cracks under axial load. The elastic modulus reflects the ability of rock to maintain cracks. Therefore, the normalized values based on Poisson's ratio and elastic modulus parameters can reflect the brittleness index of rock [10].

$$B_1 = \frac{E_n + v_n}{2} \quad (1)$$

In Equation (1), B_1 is the brittleness index calculated by the normalized elastic modulus and Poisson's ratio. The calculation formulas of E_n and v_n are as follows:

$$E_n = \frac{E - E_{min}}{E_{max} - E_{min}} \quad (2)$$

$$v_n = \frac{v_{max} - v}{v_{max} - v_{min}} \quad (3)$$

In the formula, E_n is the normalized elastic modulus; v_n is the normalized Poisson's ratio (dimensionless); E is the elastic modulus measured in laboratory experiments (MPa); v is the Poisson's ratio measured in laboratory experiments (dimensionless); E_{max} and E_{min} are the maximum elastic modulus and the minimum elastic modulus of the reservoir in the study area (MPa); v_{max} and v_{min} are the maximum Poisson's ratio and the minimum Poisson's ratio of the reservoir in the study area, respectively (dimensionless).

The method of calculating the brittleness index based on the secant modulus of the peak strength comprehensively considers the peak stress of rock in the triaxial fracturing process and the strain size during failure.

$$B_2 = \alpha \frac{\sigma_P}{\varepsilon_P} \quad (4)$$

In Equation (4), σ_P is the peak strength (MPa); ε_P is the peak strain (%); α is the model coefficient, and its value in this paper was 0.1; B_2 is a dimensionless brittleness index based on the secant modulus.

The brittleness index calculated based on the above two models is shown in Figure 8. It can be seen that there are some differences in the brittleness index calculated by the two models. The brittleness index B_1 of most cores is greater than B_2, and the brittleness index B_1 of a small number of cores is less than B_2. According to previous scholars' research, we classified the brittleness grade of tight sandstone in the Shan 1 and He 8 reservoirs in the Longdong area, and the classification table is shown in Table 3. Based on the rock brittleness classification table, in the brittleness index B_1 calculated according to the normalized values of Poisson's ratio and elastic modulus parameters, 5 cores showed a high brittleness, 11 cores showed brittleness, 3 cores showed a low brittleness, and 2 cores showed plastic characteristics. In the brittleness index B_2 calculated according to the secant modulus of the peak strength, only 2 cores showed a high brittleness, 11 cores showed brittleness, 8 cores showed a low brittleness, and only 1 core showed plastic characteristics.

Table 3. Rock brittleness classification table.

Brittleness Index	Brittleness Classification
>60	High brittleness
40–60	Brittleness
20–40	Lower brittleness
0–20	Plasticity

In order to quantitatively evaluate the brittleness characteristics of the formation rock in the study area more accurately, we comprehensively considered the brittleness indexes B_1 and B_2 based on the elastic modulus, Poisson's ratio and the secant modulus based on the peak strength, and proposed a calculation method for the comprehensive brittleness index B as follows:

$$B = \frac{B_1 + B_2}{2} \quad (5)$$

In Equation (5), B_1 is the brittleness index calculated based on the elastic modulus and Poisson's ratio. B_2 is the brittleness index calculated based on the secant modulus of the peak strength. The distribution diagram of the comprehensive brittleness index B is shown

in Figure 9. There were six cores showing a high brittleness, eight cores showing brittleness, six cores showing a low brittleness, and two cores showing plasticity.

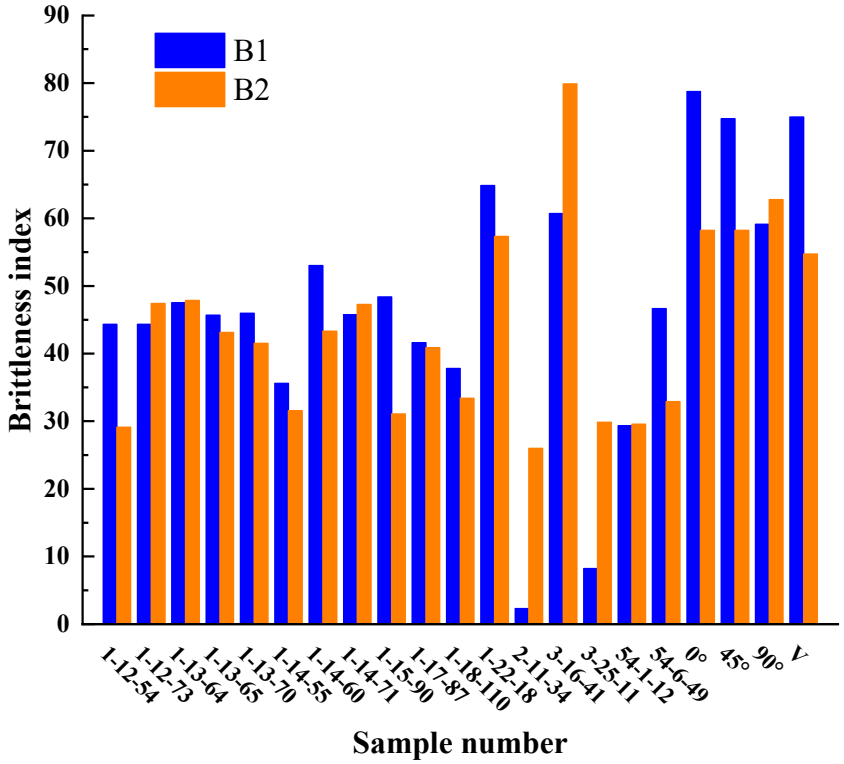

Figure 8. Distribution of brittleness index based on elastic modulus, Poisson's ratio and secant modulus based on peak strength.

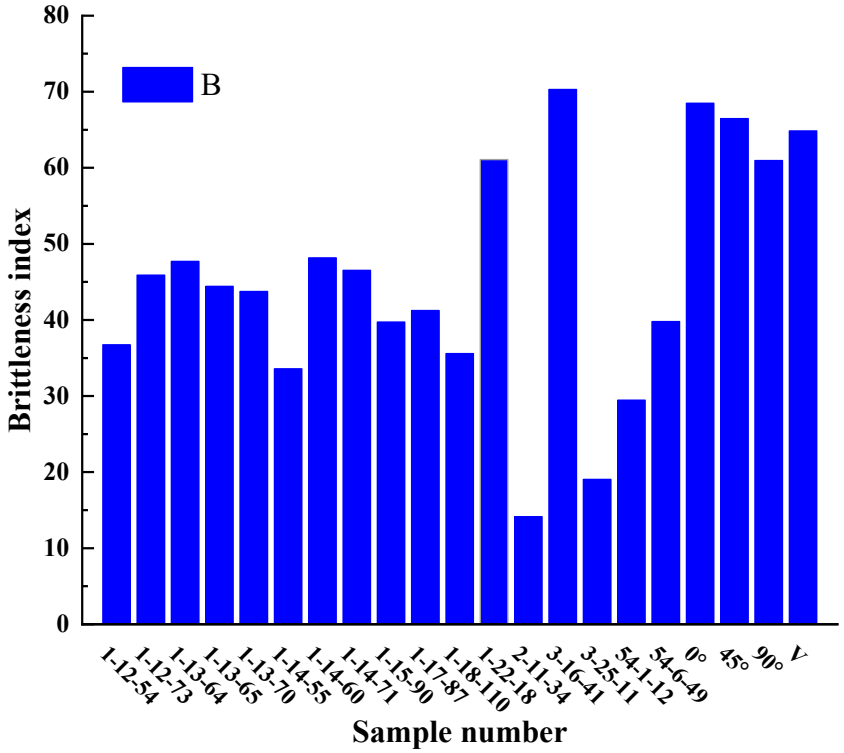

Figure 9. The distribution map of the comprehensive brittleness index calculated by the two models is comprehensively considered.

3.3. Analysis of Triaxial Compression Fracture Morphology of Sandstone with Different Brittleness Indexes and Different Coring Angles

Based on the above brittleness index calculation results, we analyzed the triaxial compression fracture morphology of different brittleness index cores in different types of sandstones. Using the CT scanning device, the core after triaxial compression was scanned. The obtained CT data volume was processed by Avizo software to obtain a three-dimensional reconstructed digital core structure. In Figure 10, the grayscale image is the original shape of the core after CT scanning, and the color image is the reconstructed digital core. Figure 10 clearly shows the fracture morphology of different cores after triaxial compression. Pebble sandstone with different brittleness indexes in Figure 10a shows a different fracture morphology. The comprehensive brittleness index of the 1-22-18 gravel sandstone was 61.08, and the comprehensive brittleness index of the 1-12-54 gravel sandstone was 36.73. The core with a high brittleness index formed the main fracture surface and secondary fracture, while the core with a low brittleness index only produced microfractures. In gray sandstone, the 1-13-70 core with a comprehensive brittleness index of 42.74 produced more secondary fractures than the 54-1-12 core with a comprehensive brittleness index of 29.44. The same rule was also seen in white sandstone. The main fracture surface of the 1-13-64 core with a comprehensive brittleness index of 47.69 was larger than that of the 2-11-34 core with a comprehensive brittleness index of 14.15, accompanied by more secondary fractures. At the same time, the failure mode of white sandstone was a typical slow dip shear failure, which is the same as the research results of Wang et al. (2020) [32]. The quartz sandstone with a comprehensive brittleness index of 70.30% produced a complex fracture network during triaxial compression, showing excellent compressibility characteristics. The experimental results show the importance of rock brittleness characteristics to fracture propagation. In order to generate complex fracture networks through fracturing in tight reservoirs, the brittleness characteristics of reservoir rocks are extremely critical influencing factors.

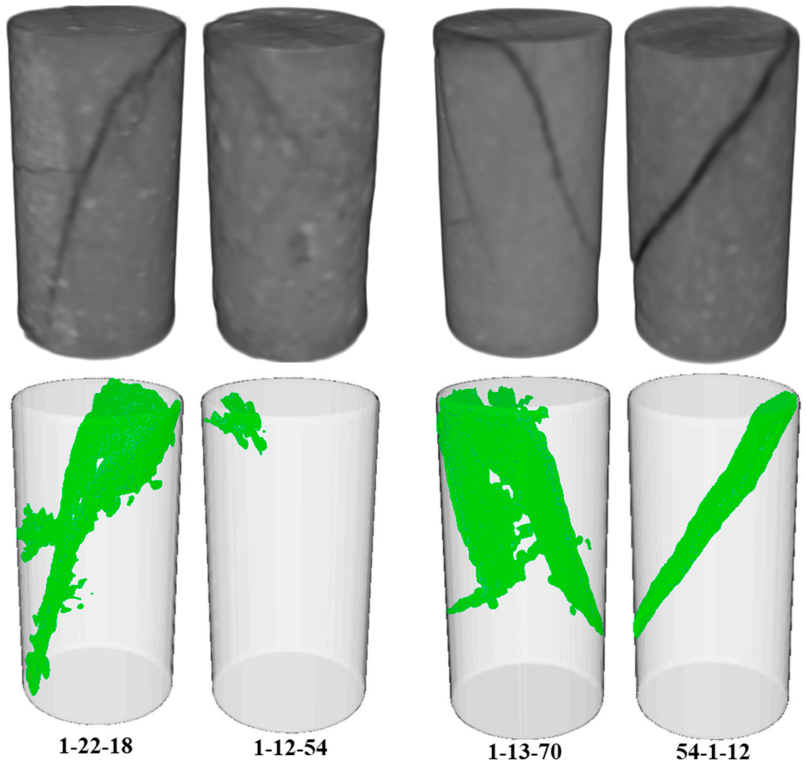

Figure 10. *Cont.*

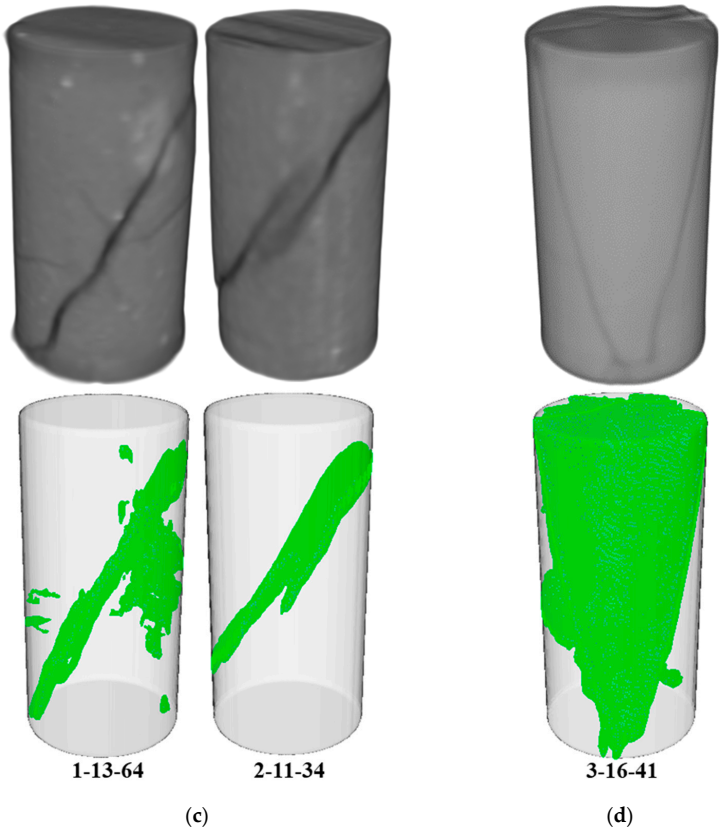

Figure 10. Triaxial compression fracture morphology of different brittle sandstones. (**a**) Fracture morphology of pebbly sandstone; (**b**) fracture morphology of gray sandstone; (**c**) fracture characteristics of white sandstone; (**d**) fracture characteristics of quartz sandstone.

Figure 11 shows the triaxial compression fracture morphology of sandstone with different coring angles in the same downhole formation. According to the calculation results of the comprehensive brittleness index, the brittleness index of sandstone with four coring angles was not much different, but different fracture morphologies were also produced during the triaxial compression process. The core sampled perpendicular to the formation produced two branch fractures. The complexity of the fracture morphology of the core parallel to the formation of 45° and 90° was higher than that of the core parallel to the formation of 0°. The reason for this phenomenon may be that the anisotropy of formation deposition and development and the different microstructures and pore structures in the core obtained by different coring angles lead to the uneven distribution of stress in triaxial compression, thus causing different fracture morphologies. Therefore, in the actual fracturing construction process, in addition to considering the brittleness characteristics of reservoir rocks, the anisotropy of formation sedimentary development is also a factor to be considered.

3.4. Study on Fracture Propagation Law of Hydraulic Fracturing in Different Brittle Cores

The fracture morphology and other information were obtained after CT scanning and the Avizo treatment of the fractured rock samples. Figure 12 shows the two-dimensional CT slices of the #1 sample with a brittleness index of 14.15 and the #2 sample with a brittleness index of 70.30 after hydraulic fracturing. It can be seen from the figure that the sample with a low brittleness index only produces a hydraulic fracture at the heel end of the perforation, and the fracture expands almost parallel to the perforation cluster. There is a natural fracture at the toe end of the perforation, but the natural fracture is not activated during the fracturing process. The three perforation clusters of the sample with a high brittleness index are all cracked, and the right end of the hydraulic fracture IF2 is repelled

by adjacent fractures, which is almost parallel to the expansion of hydraulic fractures IF1 and IF3. Due to the influence of natural fracture NF1, the left end of hydraulic fractures IF1 and IF2 extends towards the natural fracture, and natural fracture NF2 is far from the perforation cluster, so it fails to communicate effectively [33,34]. Wu et al. (2023) obtained through fracturing physical simulation tests that the higher the rock compressibility index, the easier it was to form artificial fractures with a complex morphology, which is consistent with the experimental conclusions of this study [35].

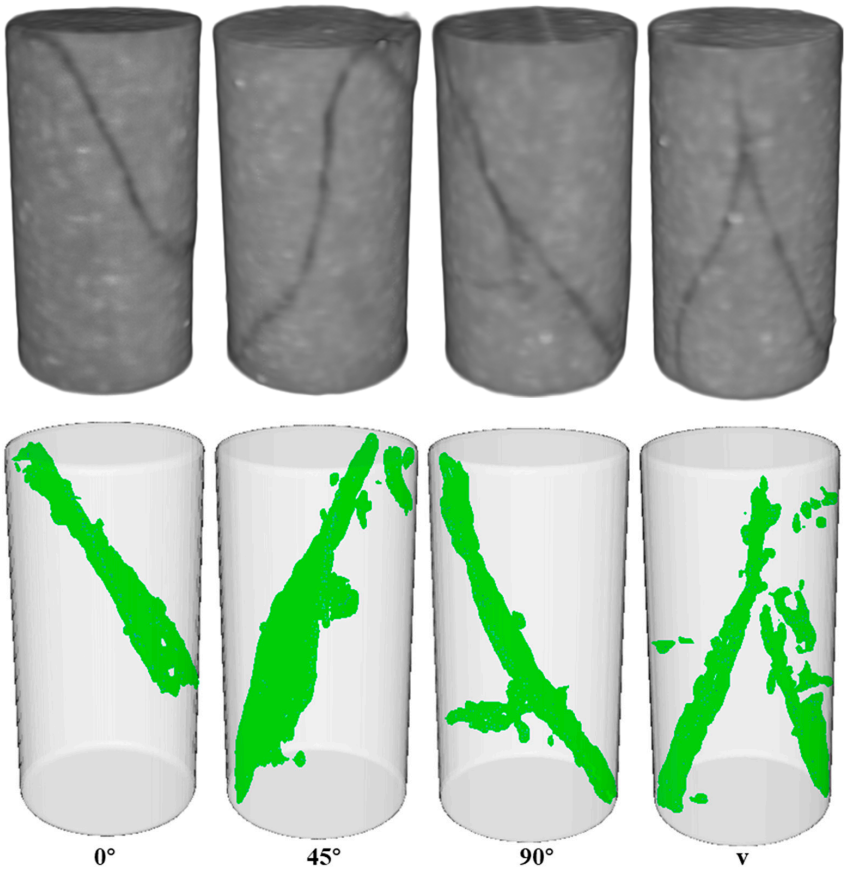

Figure 11. Triaxial compression fracture morphology of sandstone with different coring angles.

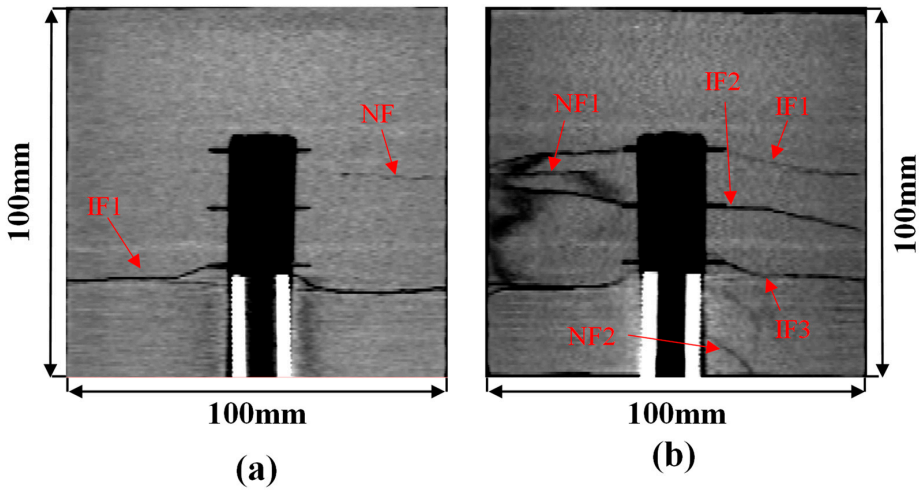

Figure 12. CT scanning slices of rock samples with different brittleness indexes after fracturing; (**a**) #1; (**b**) #2.

Figure 13 shows the injection pressure curves of #1 and #2 during fracturing. The injection pressure curve of the #1 sample is relatively simple. With the increase in injection time, the injection pressure increases to 12 MPa and then drops rapidly, indicating that the pressure is released as the fracture expands to the boundary, and then the extended pressure along the fracture of about 4 MPa tends to be stable. The injection pressure curve of the #2 sample is more complex. In the injection time of 800 s, multiple peak pressures were generated, and the peak pressure reached 37 MPa. The formation of multiple peak pressures indicates the generation of new cracks, which corresponds to the three perforation clusters of the previous CT scan two-dimensional slice.

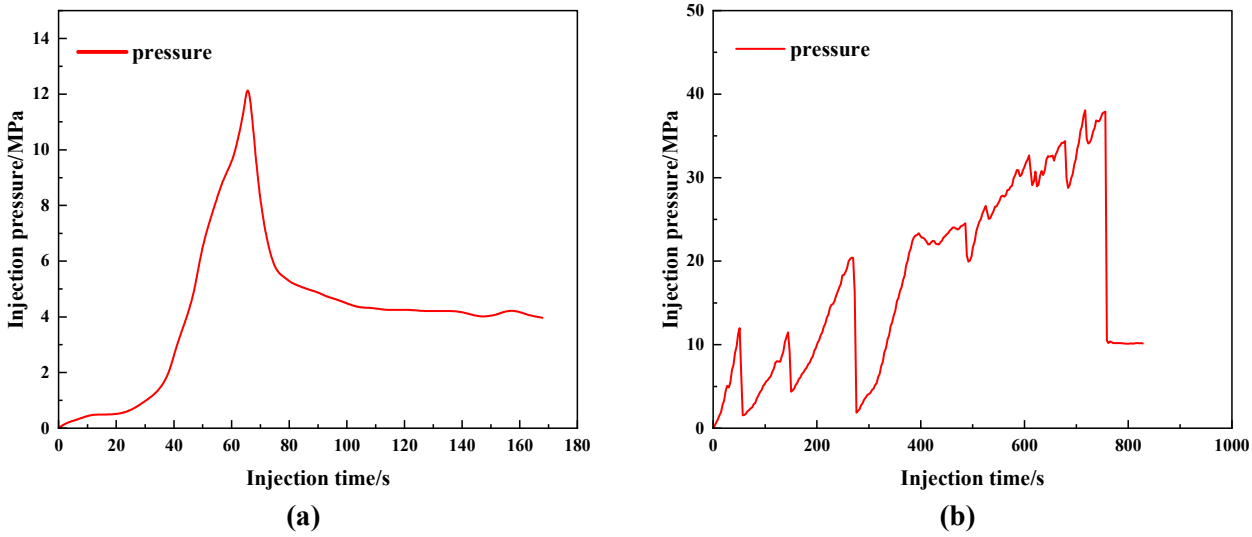

Figure 13. Injection pressure curves of rock samples with different brittleness indexes during the fracturing process; (**a**) #1; (**b**) #2.

Figure 14 shows the digital core images reconstructed by CT scanning after #1 and #2 fracturing. The #2 rock sample with a high brittleness index forms a complex fracture network during the fracturing process, and the hydraulic fracturing effect is better. The #1 rock sample with a low brittleness index has only one crack in the heel perforation cluster after fracturing, and the overall fracturing effect is poor. At the same time, we quantitatively calculated the fracture volume. The fracture volume of #1 sample was 10,025.47 mm^3, and the fracture volume of #2 sample was 43,112.34 mm^3. The fracture volume of the high brittleness index sample was close to four times that of the low brittleness index sample. The experimental conclusion has important guiding significance for the on-site hydraulic fracturing construction of tight-sandstone reservoirs in the Longdong area of the Changqing oilfield. The selection of hydraulic fracturing construction in reservoirs with good brittleness characteristics can greatly improve the fracture initiation efficiency, form a complex fracture network near the wellbore, and greatly increase the production of tight oil [36–38].

Hydraulic fracturing is to create oil–water high-speed seepage channels through physical methods to improve oil recovery. After hydraulic fracturing, the complex artificial fracture network increases the contact area between the fracturing fluid and the matrix area, which provides a chemical method to further improve oil recovery. In future research, we will further carry out research on the feasibility in this area.

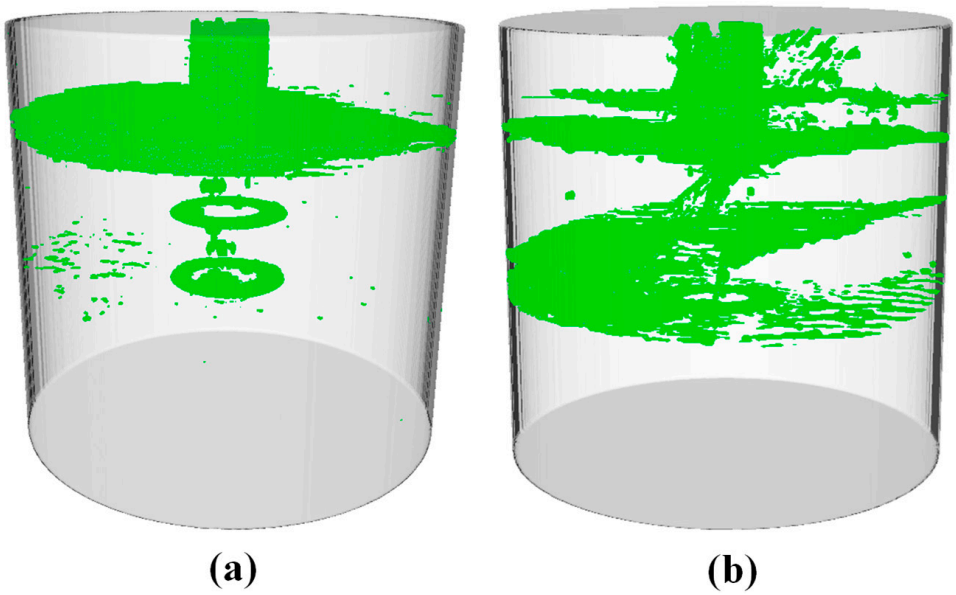

Figure 14. Three-dimensional reconstruction of the digital core by CT scanning after the fracturing of rock samples with different brittleness indexes; (**a**) #1; (**b**) #2.

4. Conclusions

Different types of sandstones exhibit great differences in the yield stage and the failure stage, and the mineral composition and natural fractures have a great influence on the brittleness characteristics. There are differences in peak strength and fracture morphology of sandstone with different coring angles due to geological heterogeneity.

There are some differences in the brittleness index calculated by the normalized numerical model based on Poisson's ratio and elastic modulus parameters and the secant modulus model based on peak strength. The comprehensive brittleness index considering the two models proposed in this paper has a high reliability.

The fracture morphology of the sample with a brittleness index of 70.30 is more complex than that of the sample with a brittleness index of 14.15 in the process of triaxial compression and hydraulic fracturing. The research conclusion shows the importance of brittleness index to on-site fracturing construction. Reservoirs with a high brittleness index can form a complex fracture network and improve single-well production.

Author Contributions: C.Z.: conceptualization, methodology, writing—original draft; Z.S.: investigation, supervision, data curation, writing—review and editing; Y.X.: investigation, English and grammar; G.H.: English and grammar; D.K.: investigation; M.L.: resources, supervision, funding acquisition. All authors have read and agreed to the published version of the manuscript.

Funding: The authors would like to acknowledge the financial support from National Natural Science Foundation of China (No. 52174045).

Data Availability Statement: Due to privacy or moral limitations, data can be provided on request. The data provided in this study can be obtained at the request of the correspondents. Due to the privacy and confidentiality of the data, the data is not public.

Conflicts of Interest: The authors declare that they have no known competing financial interest or personal relationships that could have appeared to influence the work reported in this paper.

References

1. Wang, H.; Zhao, W.; He, H.; Feng, J. Study on the characteristics of tight oil reservoirs in Longdong area of Ordos Basin-Taking Chang 7 section of Ordos Basin as an example. *Unconv. Oil Gas* **2019**, *6*, 42–51.
2. Gao, Y.; Wen, Z.; Li, W. Geochemical characteristics of lacustrine organic-rich fine-grained sedimentary rocks and their effects on tight oil and gas accumulation-Taking Chang 7 Member of Yanchang Formation in Longdong area of Ordos Basin as an example. *Nat. Gas Geosci.* **2019**, *30*, 729–739.

3. Zhang, R.; Lin, B. Compressibility evaluation of heterogeneous ultra-heavy oil unconsolidated sandstone reservoir. *Xinjiang Oil Gas* **2023**, *19*, 57–64. [CrossRef]
4. Duan, Z.; Xia, H.; Wang, L.; Gao, W.; Fan, Q.; Shi, W. Reservoir characteristics and controlling factors of Shan 1 member in Qingyang gas field, Ordos Basin. *Xinjiang Pet. Geol.* **2022**, *43*, 285–293.
5. Ma, S.; Wei, L.; Zhao, F.; Yin, X.; Chen, H. Sandstone provenance analysis of the lower 8th member of Shihezi Formation in the southern Ordos Basin. *J. Xi'an Pet. Univ.* **2023**, *38*, 1–11.
6. Sun, J.; Hao, S.; Zhao, Q.; Luo, T.; Jiang, L.; Gao, C.; Guo, C.; Yin, J.; Liu, G.; Xu, J. Shale gas reservoir characteristics and key technologies for exploration and development of Permian Shanxi Formation 1 in Yan'an area. *China Pet. Explor.* **2022**, *27*, 110–120.
7. Yu, C.; Dong, F.; Qu, K.; Jia, Y.; Guo, Q.; Bai, L. Analysis of diagenesis and diagenetic evolution sequence of Upper Paleozoic Shan 1-He 8 reservoir in Sulige 25 and 76 blocks. *Mud Logging Eng.* **2023**, *34*, 109–116.
8. Wang, X.; Xiao, D.; Wei, Y.; Wu, H. Reservoir compressibility evaluation of Tamulangou Formation in Hailar Basin. *Pet. Geol. Eng.* **2022**, *36*, 106–110, 114. [CrossRef]
9. Chen, Y.; Zhai, M. Complexity analysis of hydraulic fractures in tight glutenite reservoirs based on core brittleness characteristics. *Pet. Geol. Recovery Factor* **2020**, *27*, 33–43. [CrossRef]
10. Wang, Y.; Liang, L.; Zou, Z.; Liu, X.; Zhang, J.; Zhang, W. Analysis of brittleness characteristics and influencing factors of conglomerate in Baikouquan Formation in Mahu Sag. *Technol. Eng.* **2022**, *22*, 10544–10549. [CrossRef]
11. Cui, G.; Lu, F.; Wang, S.; Hu, R.; Wang, C. Classification and evaluation of tight sandstone reservoirs in He 8 member of Longdong area. *Pet. Geol. Eng.* **2021**, *35*, 44–49. [CrossRef]
12. Yingtao, L.I.; Zhixing, R.U.; Shang, D.E.; Huixi, L.I.; Jun, H.A.; Jibiao, Z.H.; Cheng, H.U. Experimental evaluation of natural fractures in deep carbonate reservoirs in Shunbei, Tarim Basin and its significance for oil and gas. *Pet. Exp. Geol.* **2023**, *45*, 422–433. [CrossRef]
13. Wei, Y.; Zhao, D.; Jiao, W.; Zhang, H. Heterogeneity characteristics of mechanical brittleness of deep shale reservoirs in Wufeng Formation-Longmaxi Formation in western Chongqing area-Taking well Z-3 as an example. *Unconv. Oil Gas* **2021**, *8*, 67–76.
14. Shi, S.; Zou, Y.; Wang, J.; Zhang, S.; Li, J.; Zhang, X. Reservoir brittleness characteristics of Lucaogou Formation in Jimsar Sag. *Xinjiang Pet. Geol.* **2022**, *43*, 169–176.
15. Xiao, L. Brittleness characteristics of tight reservoirs in the second member of Yingtai gas field. *Pet. Knowl.* **2022**, *3*, 54–55.
16. Mei-ben, G.A.; Tian-bin, L.I.; Guo-qing, C.H.; Lu-bo, M.E.; Chun-chi, M.A.; Yan, Z.H.; Hong-yu, Y.I.; Yu-yi, Z.H. Brittleness evaluation method based on pre-peak cracking and post-peak characteristics of rock. *Chin. J. Geotech. Eng.* **2022**, *44*, 762–768. [CrossRef]
17. Meng, F.; Wong, L.N.Y.; Zhou, H. Rock brittleness indices and their applications to different fields of rock engineering: A review. *J. Rock Mech. Geotech. Eng.* **2021**, *13*, 221–247. [CrossRef]
18. Li, H.; Huang, B.; Zhao, X.; Wu, Z.; Han, X.; Jiao, X.; Sun, Z. Experimental investigation on proppant transport and distribution characteristics in coal hydraulic fractures under true triaxial stresses. *J. Pet. Sci. Eng.* **2022**, *218*, 110993. [CrossRef]
19. Yu, B.; Liu, C.; Chen, W.; Lu, J.; Liu, Y. Experimental study on deformation and fracture characteristics of coal under different true triaxial hydraulic fracture schemes. *J. Pet. Sci. Eng.* **2022**, *216*, 110839. [CrossRef]
20. Li, M.; Zhou, F.; Sun, Z.; Dong, E.; Zhuang, X.; Yuan, L.; Wang, B. Experimental study on plugging performance and diverted fracture geometry during different temporary plugging and diverting fracturing in Jimusar shale. *J. Pet. Sci. Eng.* **2022**, *215*, 110580. [CrossRef]
21. Li, M.; Zhou, F.; Dong, E.; Zhang, G.; Zhuang, X.; Wang, B. Experimental study on the multiple fracture simultaneous propagation during extremely limited-entry fracturing. *J. Pet. Sci. Eng.* **2022**, *218*, 110906. [CrossRef]
22. Li, M.; Zhou, F.; Liu, J.; Yuan, L.; Huang, G.; Wang, B. Quantitative investigation of multi-fracture morphology during TPDF through true tri-axial fracturing experiments and CT scanning. *Pet. Sci.* **2022**, *19*, 1700–1717. [CrossRef]
23. Kong, X.; Yan, R.; Zhang, S.; Yuan, Q.; Chen, Q.; Xu, H. Fracturing initiation and propagation simulation experiments of true triaxial large-scale physical model hydraulic fracturing. *Pet. Nat. Gas Chem. Ind.* **2023**, *52*, 97–102. [CrossRef]
24. Jin, Z.; Sun, Y.; Bao, M.; Qiao, C.; Wang, Z. Experimental study on fracture propagation law of temporary plugging fracturing based on true triaxial fracturing physical simulation system. *Unconv. Oil Gas* **2021**, *8*, 98–105. [CrossRef]
25. Sun, Z.; Li, M.; Yuan, S.; Zhou, F.; Fei, R. The effect of the fracture geometries from different stratification angle on the imbibition recovery of Jimusar shale oil: A comprehensive experimental study. *Geoenergy Sci. Eng.* **2023**, *229*, 212067. [CrossRef]
26. Sun, X.; Li, E.; Duan, J.; Pu, S.; Tan, Y.; Han, Y. Research on acoustic emission characteristics and damage evolution of Beishan granite under triaxial compression. *Chin. J. Rock Mech. Eng.* **2018**, *37*, 4234–4244.
27. Gao, Y.; Guo, P.; Li, X.; Li, Y.; Xu, D.; Zou, Z.; Qin, J.; Shi, G.; Li, S. Research on triaxial compression deformation, fracture and acoustic emission characteristics of different types of reservoir rocks. *J. Eng. Geol.* **2022**, *30*, 1169–1178.
28. Shi, X.; Wang, M.; Wang, Z.; Wang, Y.; Lu, S.; Tian, W. A brittleness index evaluation method for weak-brittle rock by acoustic emission technique. *J. Nat. Gas Sci. Eng.* **2021**, *95*, 104160. [CrossRef]
29. Zou, Y.; Zhang, S.; Ma, X.; Zhang, X.; Zhang, S. Hydraulic fracture morphology and conductivity of continental shale under the true-triaxial stress conditions. *Fuel* **2023**, *352*, 129056. [CrossRef]
30. Zhu, H.; Gong, D.; Zhang, B. A new method for multi-scale 'geological-engineering' double dessert evaluation of tight sandstone gas reservoirs. *Nat. Gas Ind.* **2023**, *43*, 76–86.
31. Yuan, H.; Deng, X.; Du, H.; Yu, Y.; Xu, F. Heterogeneity characterization method of tight sandstone reservoir in Shanxi Formation outcrop of Permian in Liujiang Basin. *Pet. Nat. Gas Geol.* **2023**, *44*, 468–479.

32. Wang, Y.; Su, H.; Wang, L.; Jiao, H.; Li, Z. Comparative analysis of deformation and strength characteristics of three kinds of sandstone. *Coal J.* **2020**, *45*, 1367–1374.
33. Yang, L.; Sheng, X.; Zhang, B.; Yu, H.; Wang, X.; Wang, P.; Mei, J. Propagation behavior of hydraulic fractures in shale under triaxial compression considering the influence of sandstone layers. *Gas Sci. Eng.* **2023**, *110*, 204895. [CrossRef]
34. Zhang, J.; Xie, Z.; Pan, Y.; Tang, J.; Li, Y. Synchronous vertical propagation mechanism of multiple hydraulic fractures in shale oil formations interlayered with thin sandstone. *J. Pet. Sci. Eng.* **2023**, *220*, 111229. [CrossRef]
35. Wu, B.; Peng, C.; Wu, G.; Lou, Y.; Yin, B. Study on the influence of compressibility index on the propagation law of fracturing cracks-taking LF oilfield in the South China Sea as an example. *Oil Drill. Technol.* **2023**, *51*, 105–112.
36. Li, M.; Zhou, F. Multi-fracture initiation sequence and breakdown pressure in horizontal wells during TDPF: A visualization experimental investigation based on PMMA. *J. Pet. Sci. Eng.* **2022**, *215*, 110645. [CrossRef]
37. Zhang, Y.; Long, A.; Zhao, Y.; Zang, A.; Wang, C. Mutual impact of true triaxial stress, borehole orientation and bedding inclination on laboratory hydraulic fracturing of Lushan shale. *J. Rock. Mech. Geotech. Eng.* **2023**. [CrossRef]
38. Xie, R.; Zhou, W.; Liu, C.; Yin, S.; Radwan, A.E.; Lei, W.; Cai, W. Experimental investigation on dynamic and static rock mechanical behavior, failure modes, and sequences of frequent interbedded sand and shale reservoirs. *Interpretation* **2022**, *10*, SF23–SF36. [CrossRef]